Eur. Phys. J. C 25, 353–360 (2002)
Digital Object Identifier (DOI) 10.1007/s10052-002-1033-8

THE EUROPEAN PHYSICAL JOURNAL C

Pion correlations and resonance effects in $\bar{\mathrm{p}}\mathrm{p}$ annihilation to $4\pi^0$ at rest

O. Kortner[1], M.P. Locher[2,3], V.E. Markushin[2], P. Weber[4], O. Wigger[2,3]

[1] Ludwig–Maximilians–Universität, 80799 München, Germany
[2] Paul Scherrer Institut (PSI), 5232 Villigen, Switzerland
[3] University of Zürich, 8006 Zürich, Switzerland
[4] ETH-IPP Zürich, 8093 Zürich, Switzerland

Received: 26 February 2002 / Revised version: 22 July 2002 /
Published online: 30 August 2002 –

Abstract. We study $\pi^0\pi^0$ correlations in the exclusive reaction $\bar{\mathrm{p}}\mathrm{p} \to 4\pi^0$ at rest with complete reconstruction of the kinematics for each event. The inclusive distribution is fairly flat at small invariant mass of the pion pair while a small enhancement in the double differential distribution is observed for small invariant masses of both pion pairs. Dynamical models with resonances in the final state are shown to be consistent with the data while the stochastic HBT mechanism is not supported by the present findings.

1 Introduction

Nucleon-antinucleon annihilation into multi-pion states offers the possibility of studying Bose-Einstein (BE) correlations under controlled conditions. While the study of BE correlations in *inclusive* distributions in $N\bar{N}$ annihilation in the conventional Hanbury-Brown–Twiss (HBT) framework [1] has a long history [2–4], the use of *exclusive* distributions is relatively new. The first steps in this direction were made in [5,6] where the exclusive reactions $\bar{\mathrm{p}}\mathrm{p} \to 2\pi^+2\pi^-$ and $\bar{\mathrm{p}}\mathrm{p} \to 2\pi^+2\pi^-\pi^0$ at rest were studied on the basis of minimum bias CPLEAR data. For these data, the complete kinematical reconstruction of each event allows the direct determination of the square of the reaction amplitude and the dynamics of the BE correlations is not obscured by integration over spectators and the usage of conventional reference samples.

The present paper extends the analysis of the exclusive distributions for the $\bar{\mathrm{p}}\mathrm{p}$ annihilation at rest to the case of the $4\pi^0$ final state on the basis of the Crystal Barrel (CB) data. An appealing property of the $4\pi^0$ channel is that there are no ρ mesons, which strongly affect the final states with charged pions. Therefore the comparison of the $\pi^0\pi^0$ correlations with the charged pion correlations can clarify the origin of the signals observed.

The HBT mechanism [1], which is based on pion emission with stochastic phases over an extended emission volume, predicts an *enhancement* of like sign pion pairs at low relative momentum Q^2. This kind of enhancement seen for $\pi^+\pi^+$ and $\pi^-\pi^-$ pairs in many reactions is usually called a BE signal. For the first time in an annihilation reaction, the *inclusive* $2\pi^0$ pair distribution for $\bar{\mathrm{p}}\mathrm{p} \to 4\pi^0$ shows no such enhancement contrary to the case of $\bar{\mathrm{p}}\mathrm{p} \to 2\pi^+2\pi^-$ [5] where a weak enhancement was seen in the corresponding $\pi^+\pi^+$ and $\pi^-\pi^-$ distributions. In the double differential distribution, which is a more sensitive observable, a small enhancement is seen in the kinematical region where the $4\pi^0$ system forms two pion pairs, both having small invariant masses. As we shall discuss, the strength and the shape of the signal for the differential correlations do not favor an interpretation in terms of the conventional HBT picture of BE correlations. This conclusion is based on simulations of resonance production in the $4\pi^0$ final state which qualitatively explain the observed effects.

The plan of the paper is as follows. In Sect. 2 we describe the analysis of the data and the results for the single variable distributions. In Sect. 3, the formalism of double differential distributions is recapitulated. Section 4 presents detailed model calculations for the dominant resonance mechanisms which are compared to the data. Partial projections similar to the analysis performed earlier in the $2\pi^+2\pi^-$ case are shown as well and confronted with our dynamical model. Section 5 gives a summary and conclusions.

2 Analysis of the $4\pi^0$ data

The Crystal Barrel experiment [8,9] at the Low Energy Antiproton Ring (LEAR) at CERN was conceived for high statistics meson spectroscopy. The setup relevant for the present study used a cylindrical detector consisting of a hydrogen gas target, tracking chambers for charged particles (proportional and jet-drift-chambers), and an electromagnetic calorimeter with 1380 CsI crystals of 16 radiation lengths each for the detection of photons. The calorimeter is surrounded by a 1.5 T solenoid magnet.

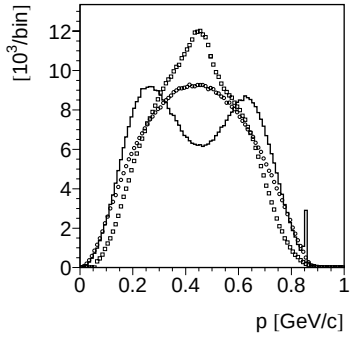

Fig. 1. The measured single-pion momentum distribution $dN_\pi/d|\mathbf{p}_\pi|$ for the $4\pi^0$ channel (thick histogram). The pure phase space distribution is shown with ∘ and the single-pion momentum distribution for the $2\pi^+2\pi^-$ channel [5] with □

2.1 Event selection

The $4\pi^0$ data analyzed in this study was taken by Crystal Barrel in November 1994 using antiprotons stopped in the hydrogen gas target at 1.2 MPa with the zero prong trigger, see [8]. Offline, the data was subjected to the following selection criteria:

- exactly 8 photon energy deposits (PED) in the calorimeter;
- no PED adjacent to the beam pipe (risk of missing energy);
- no $\bar{p}$ pileup condition;
- no charged tracks in proportional chambers or jet-drift-chambers (eliminates backscatters, trigger inefficiency, and pair production);
- no PED below 20 MeV(suppresses split-offs);
- total momentum between 0 and 200 MeV/c, and total energy $m_{\bar{p}p} \pm 173$ MeV/c^2.

For this set of events, a kinematic fit is performed and the most likely photon combinations are chosen. Combinatorial background is determined by simulation to be of the order of 18 percent. The photon energy resolution is $\sigma_E/E = 2.5\%/\sqrt[4]{E/\mathrm{GeV}}$.

The measured single pion inclusive momentum distribution is plotted in Fig.1. The shape of the π^0 momentum distribution differs significantly from phase space due to the strong production of resonances in the mass region between 1.2 GeV and 1.7 GeV as discussed in [10] and in Sect. 4. Theoretical simulations of the according decay distributions show that the broad peak at 0.2 GeV/c is due to pions recoiling with small energies against a heavy resonance like $a_2(1660)$ or $\pi_2(1670)$, while the maximum around 0.65 GeV/c stems from the decay of lighter resonances like $f_2(1270) \to 2\pi^0$ and maybe $\pi(1300) \to 3\pi^0$ in combination with π^0 spectators. The narrow peak at 0.85 GeV/c corresponds to the $\bar{p}p \to \pi^0 + \eta_{\to 3\pi^0}$ decay. For comparison we show the single–pion distribution for the $2\pi^+2\pi^-$ channel from [5] in Fig. 1 as well (the $2\pi^+2\pi^-$ state is dominated by other resonances, in particular, ρ^0, leading to a different structure in the distribution). We shall discuss resonance production models in detail in Sect. 4.

2.2 Correlation functions for inclusive distributions

For the benefit of the reader, we summarize below the standard BE formalism according to [5]. The single-particle inclusive density $\rho_1(p_1)$ and the two-particle inclusive density $\rho_2(p_1, p_2)$ are related to the differential cross-sections by

$$\rho_1(p_1) = \sigma^{-1} \frac{d\sigma}{d^3\mathbf{p}_1/(2E_1)} \tag{1}$$

$$\rho_2(p_1, p_2) = \sigma^{-1} \frac{d\sigma}{d^3\mathbf{p}_1/(2E_1)\; d^3\mathbf{p}_2/(2E_2)} \quad . \tag{2}$$

One of the definitions of pion pair correlations is based on the formula

$$c(p_1, p_2) = \rho_2(p_1, p_2) - \rho_1(p_1)\rho_1(p_2) \quad . \tag{3}$$

Alternatively the two-particle correlations can be described in terms of the ratio

$$C(p_1, p_2) = \frac{\rho_2(p_1, p_2)}{\rho_0(p_1, p_2)} \quad , \tag{4}$$

where $\rho_0(p_1, p_2)$ is the two-particle distribution *in the absence of correlations*, with various prescriptions being used in the literature. A choice consistent with (3) is the product of the single-particle densities $\rho_0(p_1, p_2) = \rho_1(p_1)\,\rho_1(p_2)$.

Averaging over angles and momenta gives a correlation function depending on one variable, the two-pion invariant mass M:

$$C(M) = \frac{\rho_2(M)}{(\rho_1 \cdot \rho_1)(M)} \tag{5}$$

$$\rho_2(M) = \int \delta\left(M - \sqrt{(p_1+p_2)^2}\right) \times \rho_2(p_1, p_2) \frac{d^3\mathbf{p}_1 d^3\mathbf{p}_2}{(2E_1)(2E_2)} \tag{6}$$

$$(\rho_1 \cdot \rho_1)(M) = \int \delta\left(M - \sqrt{(p_1+p_2)^2}\right) \times \rho_1(p_1)\rho_1(p_2) \frac{d^3\mathbf{p}_1 d^3\mathbf{p}_2}{(2E_1)(2E_2)} \tag{7}$$

The invariant mass M is uniquely related to the square of the momentum difference:

$$(p_1 - p_2)^2 = 4\mu^2 - M^2 = -Q^2, \tag{8}$$

where μ is the pion mass and $\mathbf{Q}$ is the difference of the three-momenta of the two pions in their center-of-mass system (CMS), therefore the variables M^2 and Q^2 are equivalent.

Because of the total energy-momentum conservation, the ratio $C(M)$ is not a constant even if the distributions $d\sigma/(d^3\mathbf{p}_1/2E_1)$ and $d\sigma/(d^3\mathbf{p}_1/2E_1)(d^3\mathbf{p}_2/2E_2)$ are determined by phase space alone (see [5,6]). This effect becomes negligible for reactions at much higher energy, but it is important for annihilation at rest.

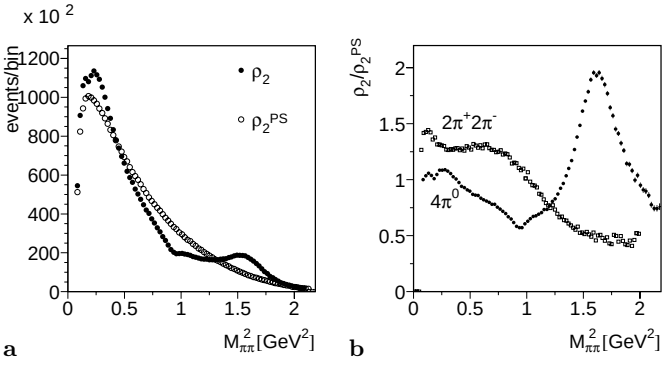

Fig. 2a,b. Inclusive two-pion correlations *vs.* the effective mass squared M^2 of the pion pair in the $4\pi^0$ channel: **a** The experimental two-particle distribution $\rho_2(M)$, (6), in comparison with the phase space distribution $\rho_2^{PS}(M)$. The simulated spectrum is normalized to the number of measured events. **b** The ratio $\rho_2(M)/\rho_2^{PS}(M)$. The $2\pi^+2\pi^-$ data are from [5]

2.3 Single-variable two-pion correlations

In this subsection we present as an introduction the single-variable two-pion correlation $C(M)$ which has been frequently used in previous analyses. In order to isolate the correlation effects we compare the experimental density with a four-pion phase space distribution corrected for experimental cuts and efficiencies in the same way as the data.

The data sample of 459803 events was used to calculate the two-particle distributions $\rho_2^{00}(M)$ defined by (6) for π^0 pairs[1], see Fig. 2a. The corresponding two-particle density from the phase space simulation is called $\rho_2^{PS}(M)$. The simulation was produced with the GEANT software [11], and subjected to the same cuts and selections as the real data. It comprises 956511 events. Figure 2b shows the ratio $\rho_2^{00}(M)/\rho_2^{PS}(M)$, for which the kinematical correlations discussed in Sect. 2.2 cancel.

An interesting feature is that this inclusive distribution shows no significant peaking at small invariant mass of the pion pair as it would be expected in the HBT model. The little structure below 0.4 GeV^2 is actually due to projected enhancement for $M^2 > 1.5$ GeV^2 as can be seen from the differential distributions in Sect. 3 further below. The peak at $M^2 = 1.6$ GeV^2 is due to $f_2 \to \pi^0\pi^0$. In Fig. 2b the inclusive distribution for the charged channel $\bar{p}p \to 2\pi^+2\pi^-$ from [5] is shown for comparison.

To study the correlation function $C(M)$ in (5), the two-particle distribution for uncorrelated pion pairs has been calculated using the same event-mixing method as in [5]. The experimental distribution $(\rho_1 \cdot \rho_1)(M)$ and the simulated distribution $(\rho_1 \cdot \rho_1)^{PS}(M)$ are plotted in Fig. 3, along with their ratio. Figure 4 shows the correlation functions $C(M)$ for the $\pi^0\pi^0$ pairs in comparison with the phase space distribution. In order to remove the trivial M-dependence which arises from the energy-momentum

[1] Here and below all distributions for $4\pi^0$ events contain multiple entries per event corresponding to all possible two–particle combinations

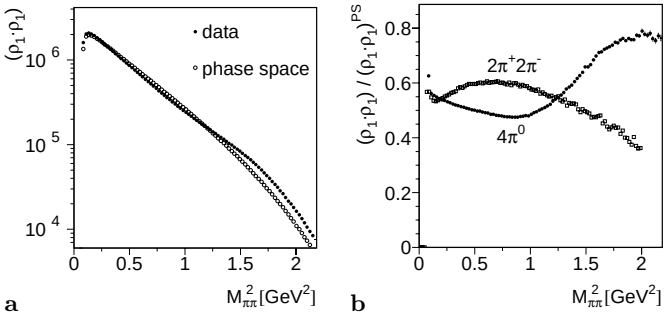

Fig. 3. a The experimental distribution $(\rho_1 \cdot \rho_1)(M)$ (•) and the phase space distribution $(\rho_1 \cdot \rho_1)^{PS}(M)$ (∘) obtained by mixing events. **b** The ratio $(\rho_1 \cdot \rho_1)(M)/(\rho_1 \cdot \rho_1)^{PS}(M)$. The simulated spectrum is normalized to the number of measured events. The $2\pi^+2\pi^-$ data are from [5]

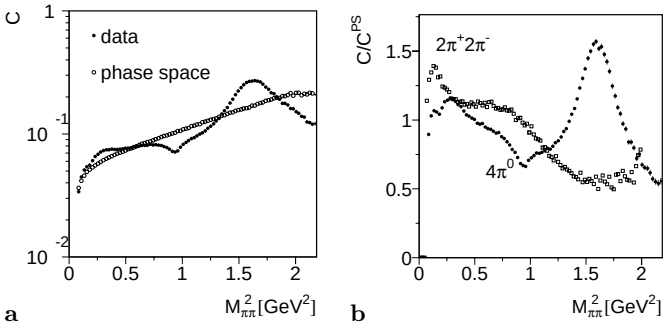

Fig. 4. a The experimental correlation function $C(M)$, (5), *vs.* the square of the effective mass M^2 of two pions in the $4\pi^0$ channel (•) in comparison with the corresponding phase space correlation function (∘). **b** The experimental correlation function normalized to the phase space distribution, $C(M)/C^{PS}(M)$, (9). The $2\pi^+2\pi^-$ data are from [5]

conservation, (5-7), and the influence of the experimental cuts, the following double ratio has been calculated:

$$\frac{C(M)}{C^{PS}(M)} = \frac{\rho_2(M)}{(\rho_1 \cdot \rho_1)(M)} : \frac{\rho_2^{PS}(M)}{(\rho_1 \cdot \rho_1)^{PS}(M)} \quad . \qquad (9)$$

The result is shown in Fig.4b. Clearly the inclusive π^0 pair correlation function is fairly flat at small M. This is unexpected in the conventional HBT picture. It also contrasts to our findings for charged pion correlations, where the inclusive correlation function shows a weak enhancement at small M [5], see Fig.4b. For a resonance production model describing the data by means of $f_2(1270)$, $a_2(1660)$, and $\pi_2(1670)$ see Sect. 4,

3 Differential two-pion correlations

So far we have presented the inclusive correlation function $C(M)/C^{PS}(M)$ where all kinematical variables except the invariant mass M of one pion pair have been integrated out. To investigate possible correlation signals in more detail we turn to differential densities. Our approach follows

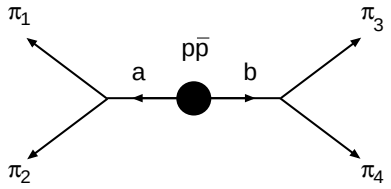

Fig. 5. The two-pion subsystems $a = (\pi_1 + \pi_2)$ and $b = (\pi_3 + \pi_4)$ in the four pion final state

the method used previously for the systems of charged pions [5,6].

The reaction $\bar{p}p \to 4\pi^0$ at rest in the CB experiment proceeds from the S-wave state $J^{PC} = 0^{-+}$ and the P-wave atomic states $J^{PC} = 0^{++}, 1^{++}, 2^{++}$. The corresponding pion distribution for the final state configuration $\{\mathbf{p}_i\},\ i = 1,2,3,4$, has the form

$$d\sigma(\{\mathbf{p}_i\}) \sim \left(w_S|T(\mathbf{k},\{\mathbf{p}_i\})|^2 + w_P|\nabla_k T(\mathbf{k},\{\mathbf{p}_i\})|^2\right)_{\mathbf{k}\to 0} \times d\Phi_4(p,p_1,p_2,p_3,p_4) = \overline{|T(\mathbf{k},\{\mathbf{p}_i\})|^2_{\mathbf{k}\to 0}}\, d\Phi_4(p,p_1,p_2,p_3,p_4) \quad . \quad (10)$$

Here $T(\mathbf{k},\{\mathbf{p}_i\})$ is the amplitude of the $\bar{p}p$ annihilation from the initial $\bar{p}p$ state with relative momentum $\mathbf{k}$, $d\Phi_4(p,p_1,p_2,p_3,p_4)$ is the 4-body relativistic phase space, and the limit $\mathbf{k} \to 0$ implies the incoherent sum[2] of the S and P-wave states with the corresponding weights w_S and w_P. The four-vectors of the pions are $p_i = (E_i, \mathbf{p}_i)$, and $p = (2m_p, 0)$ is the total four-momentum for $\bar{p}p$ annihilation at rest, m_p being the proton mass.

We introduce the two-pion subsystems a and b with four-momenta $p_a = (p_1 + p_2)$ and $p_b = (p_3 + p_4)$ and invariant masses M_a and M_b, see Fig. 5. Given the invariant masses M_a and M_b, the double differential cross section is defined by integrating over the angles specifying the relative orientation of the momenta of the pions within the subsystems a and b and the relative orientation of the subsystems a and b (the corresponding solid angles are $d\Omega_{12}$, $d\Omega_{34}$, $d\Omega_{ab}$). For the reaction $\bar{p}p \to 4\pi^0$ we have

$$\frac{d\sigma}{dM_a^2 dM_b^2} \sim W(\sqrt{s}, M_a, M_b) \int \overline{|T(\mathbf{k},\{\mathbf{p}_i\})|^2_{\mathbf{k}\to 0}} \times d\Omega_{ab} d\Omega_{12} d\Omega_{34} \quad . \quad (11)$$

Here the factor $W(M, M_a, M_b)$ is given by

$$W(M, M_a, M_b) = \frac{P_{ab}}{M}\sqrt{\left(1 - \frac{4\mu^2}{M_a^2}\right)\left(1 - \frac{4\mu^2}{M_b^2}\right)}, \quad (12)$$

$$P_{ab} = P(M, M_a, M_b) \quad , \quad (13)$$

$$P(M, M_a, M_b) = \frac{\sqrt{(M^2 - (M_a + M_b)^2)(M^2 - (M_a - M_b)^2)}}{2M} \quad (14)$$

[2] The notation $\overline{|T(\mathbf{k},\{\mathbf{p}_i\})|^2_{\mathbf{k}\to 0}}$ implies a sum over initial spin states $J^{PC} = 0^{-+}, 0^{++}, 1^{++}, 2^{++}$, and all quantum numbers specifying the initial spin and the total angular momentum are suppressed

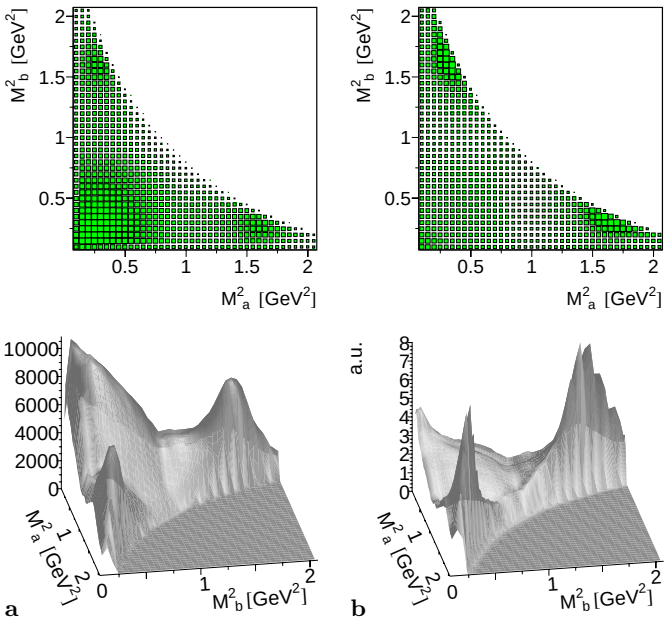

Fig. 6a,b. The double-differential distributions *vs.* the invariant masses of two π^0 pairs (6 entries per one physical event): **a** the double-differential cross section $d\sigma/dM_a^2 dM_b^2$; **b** the double-differential density $\varrho(M_a, M_b)$, (15). The box plots (top) and the surface plots (bottom) represent the same data. Both the cross section and the density plots are not corrected for acceptance. The surface plots have their origin in the rear left corner, allowing a better view of the interesting features of the data

where $P(M, M_a, M_b)$ is the relative momentum of two particles with masses M_a and M_b and the total invariant mass M, in our case $M = 2m_\mathrm{p}$. Removing the phase space factor $W(M, M_a, M_b)$, we define the double–differential density:

$$\varrho(M_a, M_b) = \frac{1}{W(M, M_a, M_b)} \frac{d\sigma}{\sigma \cdot dM_a^2 dM_b^2} \sim \int \overline{|T(\mathbf{k},\{\mathbf{p}_i\})|^2_{\mathbf{k}\to 0}}\, d\Omega_{ab} d\Omega_{12} d\Omega_{34} \quad (15)$$

where σ is the total cross section.

An advantage of using the double differential density $\varrho(M_a, M_b)$ is that it does not contain *kinematical* dependences on the invariant masses of the two-pion pairs a and b. This means that for a constant T matrix the density $\varrho(M_a, M_b)$ does not depend on its argument M_a and M_b, contrary to $\rho_2(M_a) = d\sigma/dM_a$ of (6) which unavoidably involves the phase–space dependence.

The double-differential cross-section $d\sigma/dM_a^2 dM_b^2$ corresponding to the raw data is shown in Fig. 6a, and the corresponding double differential density $\varrho(M_a, M_b)$ in Fig. 6b. These raw data must be corrected for the acceptance of the detector, which is shown in Fig. 7. The differential density $\varrho^{\mathrm{PS}}(M_a, M_b)$ is calculated using the four–pion phase space with the detector acceptance taken into account. The double differential density corrected for the detector acceptance $\varrho(M_a, M_b)/\varrho^{\mathrm{PS}}(M_a, M_b)$ is plotted in Fig. 8. Note that the double differential view shows a weak

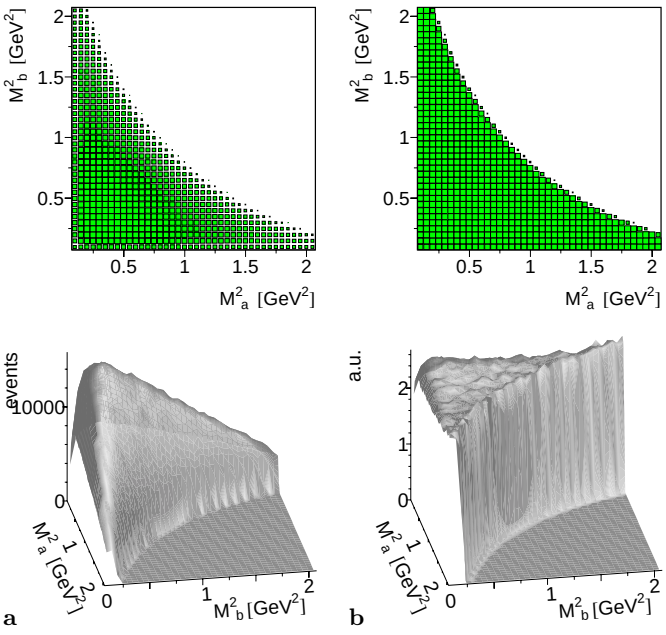

Fig. 7a,b. The acceptance simulation of the detector, calculated for events distributed uniformly in phase space: **a** the double-differential distribution $d\sigma^{\rm PS}/dM_a^2 dM_b^2$; **b** the double-differential density $\varrho^{\rm PS}(M_a, M_b)$. The box plots (top) and the surface plots (bottom) represent the same data. The surface plots have their origin in the rear left corner, allowing a better view of the interesting features of the data

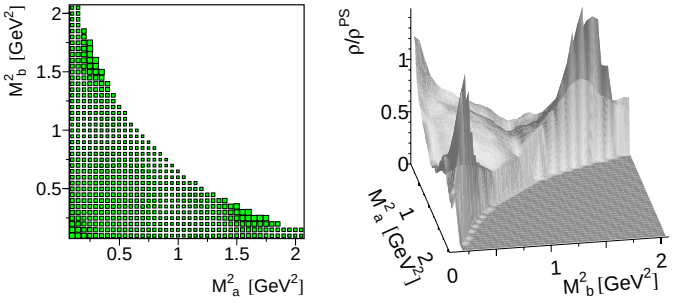

Fig. 8. The experimental double–differential density $\varrho(M_a, M_b)/\varrho^{\rm PS}(M_a, M_b)$ corrected for acceptance. Both plots represent the same data. The surface plot has its origin in the rear left corner, allowing a better view of the interesting features of the data

enhancement at low values of M^2 much weaker than in the corresponding $2\pi^+2\pi^-$ case, see Fig. 8 of [5]. On projection the enhancement is hardly visible in the inclusive distribution of Fig. 4. The enhancements for $M_b^2 > 1.4$ GeV^2 in Fig. 8 produce the little structure below 0.4 GeV^2 in Figs. 2b and 4b when the projection onto M_a^2 is made.

For the further discussion in Sect. 4 we construct the following partial projections of the two–particle density. The two–dimensional space (M_a, M_b) is divided into slices $M_i^2 \le M_b < M_{i+1}^2$ and the projections $\varrho_i(M_a)$ are defined by

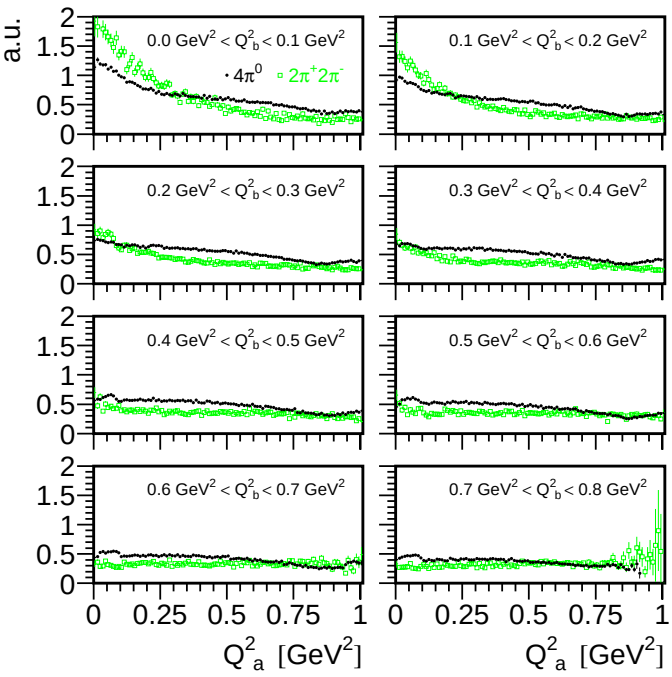

Fig. 9. The acceptance–corrected projections $\varrho_i(M_a)$ of the differential density $\varrho(M_a, M_b)/\varrho^{\rm PS}(M_a, M_b)$ for different intervals of the invariant mass of the other $\pi^0\pi^0$ pair (•). The corresponding projections for the like charge pion pairs in the $2\pi^+2\pi^-$ final state from the analysis [5] are shown for comparison (○). The relative momentum Q, (8), is used instead of the invariant mass M for the sake of convenience

$$\varrho_i(M_a) = \int_{M_i^2}^{M_{i+1}^2} \frac{\varrho(M_a, M_b)}{\varrho^{\rm PS}(M_a, M_b)}\, dM_b^2 \qquad (16)$$

The partial projections $\varrho_i(M_a)$ are plotted in Fig. 9. There is some peaking at small M_a in the first two slices hardly visible in the inclusive distributions of Fig. 4b. The slices in the mass interval 0.3 GeV$^2 \le M_b^2 \le 1.2$ GeV^2 are more or less flat. In comparison to the corresponding projections for the annihilation into $2\pi^+2\pi^-$, the observed enhancement at small Q_a^2 in the $\pi^0\pi^0$ case is weak even for the lowest interval $0.0 < Q_b^2 < 0.1$ GeV^2.

4 Discussion

4.1 Resonance effects

Resonances are strongly produced in the reaction $\bar{p}p \to 4\pi^0$, see Figs. 6 where the signals of f_2 are clearly seen in the invariant mass projections. The total spin S and the relative angular momentum L of the $\bar{p}p$ system annihilating into $4\pi^0$ are constrained by the conservation of C–parity: $C = (-1)^{L+S} = 1$. Therefore, the annihilation into $4\pi^0$ can occur in the case of the S–wave annihilation ($L = S = 0$) from the state $J^{PC} = 0^{-+}$ only, and in the case of the P–wave annihilation ($L = S = 1$) from the states $J^{PC} = 0^{++}, 1^{++}, 2^{++}$.

Following the analysis [10] of Crystal Barrel data we focus our attention on the most prominent mechanisms

seen in the $4\pi^0$ channel. For the dense gaseous target at 1.2 MPa, the fractions of the total S-wave and P-wave annihilations are approximately equal to each other [15]. For the sake of simplicity, we focus our attention on one P-wave channel $J^{PC} = 2^{++}$, which has the largest statistical weight, and the S-wave channel $J^{PC} = 0^{-+}$. We do not attempt to make a global fit of the data in the $4\pi^0$ channel, which would be far beyond the scope of this paper. Rather we want to present a simple model which turns out to describe the main features of the differential data. The $a_2(1660)$ [16] used in our simulation has been seen in the earlier Crystal Barrel analysis [17] and in the reaction $\bar{p}p \to K^+K^-\pi^0$ [18]. The following mechanisms have been taken into consideration:

$$\bar{p}p(J^{PC} = 0^{-+}) \to a_2(1660) + \pi^0 \quad (17)$$
$$\searrow f_2(1270) + \pi^0$$
$$\searrow 2\pi^0$$

$$\bar{p}p(J^{PC} = 2^{++}) \to f_2(1270) + 2\pi^0 \quad (18)$$
$$\searrow 2\pi^0$$

$$\bar{p}p(J^{PC} = 2^{++}) \to a_2(1660) + \pi^0 \quad (19)$$
$$\searrow f_2(1270) + \pi^0$$
$$\searrow 2\pi^0$$

$$\bar{p}p(J^{PC} = 2^{++}) \to \pi_2(1670) + \pi^0 \quad (20)$$
$$\searrow f_2(1270) + \pi^0$$
$$\searrow 2\pi^0$$

$$\bar{p}p(J^{PC} = 2^{++}) \to \pi(1300) + \pi^0 \quad (21)$$
$$\searrow \sigma + \pi^0$$
$$\searrow 2\pi^0$$

$$\bar{p}p(J^{PC} = 2^{++}) \to \sigma + f_0 \quad (22)$$
$$\to 4\pi^0$$

$$\bar{p}p(J^{PC} = 2^{++}) \to \sigma + \sigma \quad (23)$$
$$\to 4\pi^0$$

$$\bar{p}p(J^{PC} = 0^{++}) \to \sigma + \sigma \quad (24)$$
$$\to 4\pi^0$$

$$\bar{p}p(J^{PC} = 0^{++}) \to \sigma + f_0 \quad (25)$$
$$\to 4\pi^0$$

The details of the calculations are given in Appendix A.

As a first step, we inspect the double–differential densities corresponding to each individual mechanism in order to demonstrate the effects expected if one of these mechanisms would be dominant. In reality, a coherent superposition of several mechanisms is required to describe the data [10], therefore, as a second step, we investigate the double-differential distributions corresponding to such superpositions. Our goal is to find out which of the mechanisms considered are able to describe the global features of the differential mass distributions. Once these features are established we also get a prediction for the double differential distributions near the origin from these ordinary

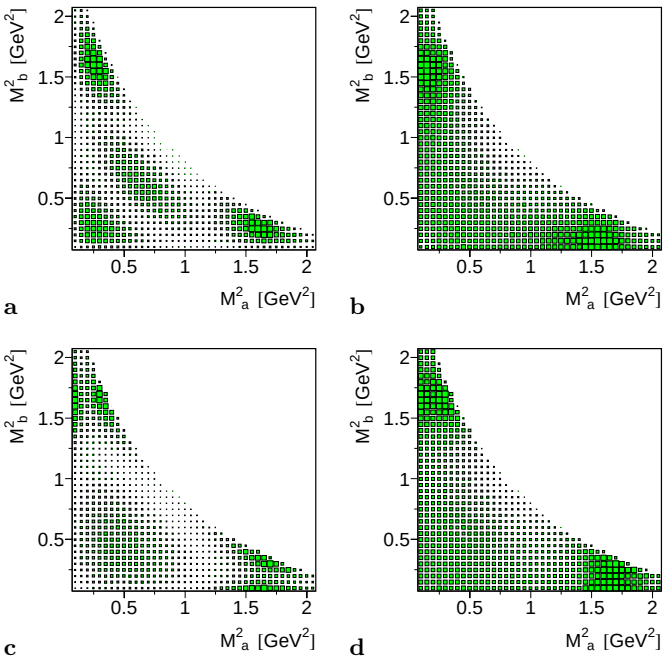

Fig. 10a–d. The double-differential density $\varrho(M_a, M_b)$ calculated for different reaction mechanisms: **a** $\bar{p}p(J^{PC} = 0^{-+}) \to a_2(1660)_{\to f_2(1270)+\pi^0} + \pi^0$, **b** $\bar{p}p(J^{PC} = 2^{++}) \to f_2(1270) + 2\pi^0$, **c** $\bar{p}p(J^{PC} = 2^{++}) \to a_2(1660)_{\to f_2(1270)+\pi^0} + \pi^0$, **d** $\bar{p}p(J^{PC} = 2^{++}) \to \pi_2(1670)_{\to f_2(1270)+\pi^0} + \pi^0$.

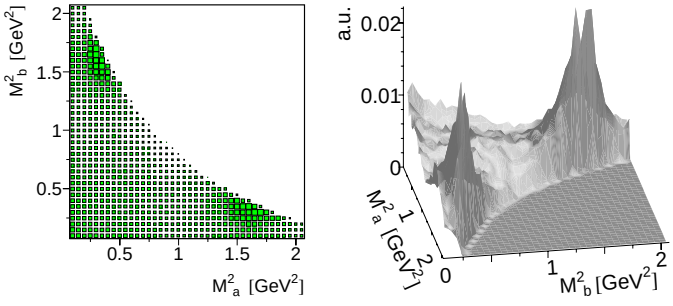

Fig. 11. The double-differential density $\varrho(M_a, M_b)$ calculated for a sum of the mechanisms (18-20) as discussed in the text. The surface plot has its origin in the rear left corner, allowing a better view of the interesting features of the data

resonance mechanisms without introducing any HBT-like stochastic correlations.

The double–differential densities calculated for the mechanisms (17,18,19,20) are shown in Figs.10a,b,c,d.

By varying the relative weights and phases of the individual mechanisms we have found that the superpositions of the three mechanisms (18,19, and 20) are sufficient to obtain a qualitative agreement with the data:

$$T = c_1 T_{f_2(1270)+2\pi^0} + c_2 e^{i\phi_2}\, T_{a_2(1660)+\pi^0} + c_3 e^{i\phi_3}\, T_{\pi_2(1670)+\pi^0} \quad (26)$$

In fact, the main features of the data can be reproduced even with the two mechanisms (19) and (20) (note that they include the contribution from the lighter meson

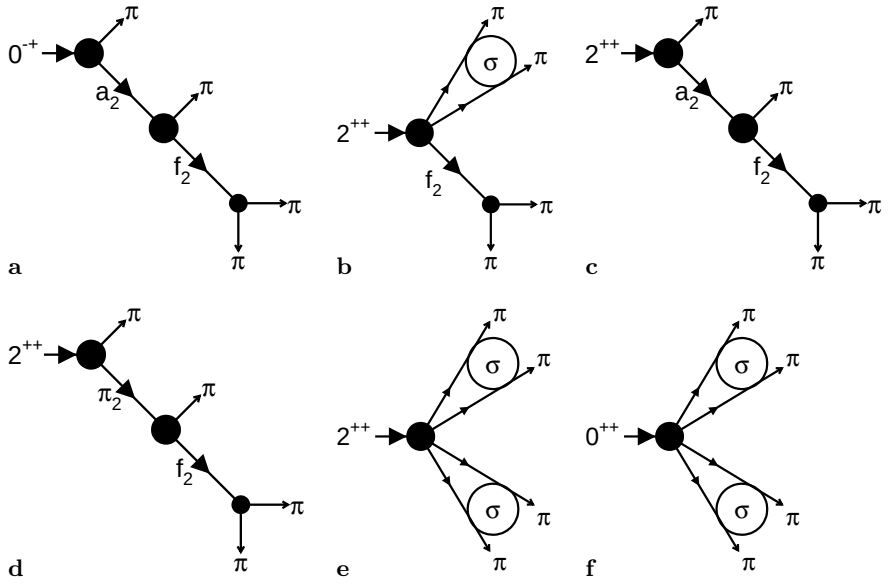

Fig. 12a–f. The resonance mechanisms

$f_2(1270)$, see Figs. 12b,c. Figure 11 shows an example corresponding to a superposition of the mechanisms (19) and (20) with $c_1 = 0$, $c_2 = 0.45$, $c_3 = 0.91$, $\phi_2 = 0$, $\phi_3 = 3\pi/2$ (all individual amplitudes are normalized to the same total yield of $4\pi^0$). We are not aiming at an optimal fit to the data in the present context, but Fig. 11 illustrates that the observed resonance peaks are consistent with a moderate enhancement near the origin. Compare this figure with the experimental distribution of Fig. 8.

5 Conclusion

For the annihilation reaction $\bar{p}p \to 4\pi^0$ at rest, the BE correlations between two neutral pions have been studied for the first time with full event reconstruction. The inclusive $2\pi^0$ correlation is fairly flat at small relative momentum while the inclusive pair correlation in the charged channel $\bar{p}p \to 2\pi^+2\pi^-$ shows a weak enhancement [5].

For the more sensitive and less model-dependent double-differential distribution, a weak peaking is observed near the origin (small invariant masses of the two neutral pion pairs). This is similar to though less pronounced than in the $2\pi^+2\pi^-$ channel.

The data of the single- and double-differential $2\pi^0$ correlations were compared to model calculations. The role of the ρ meson dominating the $2\pi^+2\pi^-$ dynamics is replaced by a model with a_2, π_2, and f_2 resonances in the $4\pi^0$ case. Resonance production explains the fairly different spectra of the two reactions. It is found that with an adequate choice of reaction amplitudes the dynamical model describes the main features of the single- and double-differential distributions, including a slight enhancement near the origin.

From this result, together with the absence of a correlation signal in the inclusive $2\pi^0$ correlation, we conclude that our analysis does not favor the interpretation of pion correlation signals in terms of an HBT-type model with stochastic pion emission phases.

Acknowledgements. The authors are very grateful to the Crystal Barrel Collaboration for making available the data. In this connection we would like to thank in particular Ulrich Wiedner and Črtomir Zupančič. We had stimulating discussions on aspects of pion correlations with Eberhard Klempt and Ulrike Thoma. One of us (MPL) would like to thank the TRIUMF theory group for hospitality during completion of this paper.

A Appendix

The amplitudes corresponding to the resonance mechanisms (18,19,20,23,17,24) are given by the diagrams in Figs. 12. The calculations are straightforward, so only some major elements are outlined here. The $\bar{p}p$ vertices are taken with a minimum number of derivatives. The vertex $\bar{p}p(J^{PC} = 2^{++}) \to a_2\pi$ has the form

$$V_{\bar{p}p(J^{PC}=2^{++})\to a_2\pi} = B_{\mu\nu} g^{\nu\gamma} T_{\gamma\delta} \epsilon^{\alpha\beta\mu\delta} (p_\pi)_\alpha (p_{a_2})_\beta \quad (27)$$

where $B_{\mu\nu}$ is the polarization tensor of the $\bar{p}p(J^{PC} = 2^{++})$ state and $T_{\gamma\delta}$ is the polarization tensor of the a_2, and p_π and p_{a_2} are the momenta of the corresponding particles. The $a_2 \to f_2\pi$ vertex has a similar structure, and the $\bar{p}p(J^{PC} = 2^{++}) \to \pi_2\pi$ is a trivial S-wave vertex. The $f_2\pi\pi$ vertex has the form

$$V_{f_2\pi\pi} = g_{f_2\pi\pi} T_{\mu\nu} q^\mu q^\nu F_{f_2\pi\pi}(m^2_{\pi\pi}) \quad (28)$$

where $g_{f_2\pi\pi}$ is the coupling constant, $T_{\mu\nu}$ is the polarization tensor of the f_2, $q = p_1 - p_2$, p_n are the pion momenta, and $F_{f_2\pi\pi}(m^2_{\pi\pi})$ is the form factor depending on the invariant mass of the $\pi\pi$ system.

The propagators corresponding to the tensor particles are given by the formula

$$G(p) = \frac{\frac{1}{2}(\Pi^{\mu\mu'}\Pi^{\nu\nu'} + \Pi^{\nu\mu'}\Pi^{\mu\nu'}) - \frac{1}{3}(\Pi^{\mu\nu}\Pi^{\mu'\nu'})}{p^2 - m_0^2 - \mathcal{M}(p^2)} \quad (29)$$

$$\Pi^{\mu\nu} = g^{\mu\nu} - p^\mu p^\nu / p^2 \quad (30)$$

where m_0 is the bare mass and $\mathcal{M}(p^2)$ is the mass operator. The mass operator for the f_2 meson corresponding to the $\pi\pi$ loop is defined by the dispersion integral:

$$\mathcal{M}(s) = \frac{1}{2\pi} \int_{4m_\pi^2}^{\infty} \frac{\Gamma(s')}{s - s'} ds' \tag{31}$$

$$\Gamma(s) = \frac{g_1^2 |F_{f_2\pi\pi}(s)|^2 k^5}{60\pi s} \tag{32}$$

where $k = k(s) = \sqrt{s/4 - m_\pi^2}$ is the relative momentum in the $\pi\pi$ system and the dipole form factor $F_{f_2\pi\pi}(s) = (1 + k(s)^2/\nu^2)^{-2}$ is used with $\nu = 1$ GeV. The parameters m_0 and $g_{f_2\pi\pi}$ are defined by the mass and the width of the f_2 meson, with the other decay channels being approximated by a constant width. The propagators of a_2 and π_2 are constructed in a similar way. The σ block in Fig.12a denotes the full Green function of the $\pi\pi$ system in the scalar-isoscalar channel; it was taken from the coupled channel model [19]. The components above are combined to construct the amplitudes for the resonance channels concerned; since the procedure is straightforward, we skip the resulting formulas involving lengthy tensor structures.

References

1. R. Hanbury-Brown, R.Q. Twiss, Phil. Mag. **45**, 633 (1954)
2. G. Goldhaber et al., Phys. Rev. Lett. **3**, 181 (1959); G. Goldhaber et al., Phys. Rev. **120**, 300 (1960)
3. G. Cocconi, Phys. Lett. B **49**, 459 (1974)
4. G.I. Kopylov, M.Y. Podgoretskii, Sov. J. Nucl. Phys. **19**, 215 (1974)
5. A. Angelopoulos et al., CPLEAR Collaboration, Europ. Phys. J. C **1**, 139 (1998)
6. A. Angelopoulos et al., CPLEAR Collaboration, Europ. Phys. J. C **6**, 437 (1999)
7. A. Angelopoulos et al., CPLEAR Collaboration, Nucl. Phys. A **655**, 218 (1999)
8. E. Aker et al., Nucl. Inst. Meth. A **321**, 69 (1992)
9. C. Amsler, Rev. Mod. Phys. **70**, 1293 (1998)
10. O. Kortner, Diplomarbeit, LMU München (1998), unpublished
11. GEANT, CERN Program Library Long Writeup W5013, CERN Computing and Network Division, 1993
12. R. Adler et al., CPLEAR Collaboration, Phys. Lett. B **267**, 154 (1991); R. Adler et al., CPLEAR Collaboration, Z. Phys. C **65**, 199 (1995)
13. R. Adler et al., CPLEAR Collaboration, Nucl. Instrum. Methods A **379**, 76 (1996)
14. R. Adler et al., CPLEAR Collaboration, Z. Phys. **C63**, 541 (1994)
15. A. Abele et al., Crystall Barrel collaboration, Nucl. Phys. A **679**, 563 (2001)
16. Review of Particle Physics, Europ. Phys. J. C **15**, 1 (2000), see p. 459
17. A. Abele et al., Crystall Barrel collaboration, Europ. Phys. J. **C8**, 67 (1999)
18. I. Uman et al., Nucl. Phys. A **692**, 302c (2001)
19. M.P. Locher, V.E. Markushin, H.Q. Zheng, Phys. Rev. D **55**, 2894 (1997)